Ionics (2019) 25:5201–5211
https://doi.org/10.1007/s11581-019-03060-y

ORIGINAL PAPER

Blending-based poly(vinylidene fluoride)/polymethyl methacrylate membrane for rechargeable lithium-ion batteries

Jiuqing Liu[1] · Meng Liu[1] · Chunfeng He[1] · Jie Li[1] · Qihou Li[1] · Cheng Wang[1] · Yang Xi[1]

Received: 5 March 2019 / Revised: 25 April 2019 / Accepted: 9 May 2019 / Published online: 22 May 2019
© Springer-Verlag GmbH Germany, part of Springer Nature 2019

Abstract

A gel polymer electrolyte based on the blending membranes of poly(vinylidene fluoride) (PVDF)/polymethyl methacrylate (PMMA) has been manufactured through the non-solvent-induced phase separation (NIPS) method. Its physical and electrochemical properties are characterized, and the blending compatibility of the PVDF/PMMA polymer is demonstrated by thermodynamic analysis. The increase in PMMA content has a great effect on surface morphologies of the PVDF/PMMA blending membranes, especially in terms of PM-3 (membrane with the weight ratio of PVDF/PMMA = 6:4). The PM-3 membrane presents satisfactory ionic conductivity (2.18 mS cm^{-1} at 26 °C), acceptable thermal stability, and superior compatibility with lithium. In addition, its cycle performance (130.7 mAh g^{-1} after circulating 200 cycles at 1 C) and rate capability (133.3 mAh g^{-1} at 4 C) are superior to those of the Celgard 2320 (PP/PE/PP) separator. It is indicated that the PVDF/PMMA blending membrane is promising for the fabrication of rechargeable lithium-ion battery.

Keywords Poly(vinylidene fluoride) · Polymethyl methacrylate · Gel polymer electrolyte · Lithium-ion battery

Introduction

Lithium-ion batteries (LIBs) with high energy density, large specific capacity, and long cycle life have been widely applied in the electronics industry. However, due to the anode capacity attenuation and high output potential difference, the safety of LIBs has been generally concerned owing to the battery ignition or even explosion. As a layer of insulation between the cathode and anode, the separator is an important component of LIBs; it works mainly in two ways: to act as an electronic insulator and to provide a lithium-ion transmission channel inside the battery. In general, an ideal separator needs to have good electrical insulation, low ionic resistance, high porosity, operable mechanical strength, electrochemical stability, and excellent electrolyte wettability [1, 2]. Polyolefin separators, which are currently widely used commercially, are based on polypropylene (PP) and polyethylene (PE) [3], although with some advantages in physical and electrochemical aspects, commercial separators are limited by the low ionic conductivity, poor compatibility with electrolytes, and severe shrinkage at high temperature [4–7], especially in terms of battery safety. This series of questions prompted researchers to reconsider the best candidates for the LIB separator. Under such circumstances, modifications based on PP/PE separators have attracted widespread attention, such as ceramic coating [8–12], electrospinning [13], and preparation of separators.

Gel polymer electrolyte (GPE) combines the safety of solid polymer electrolyte (SPE) with the high ionic conductivity of liquid electrolyte [14], which is considered to be a promising alternative to liquid electrolyte. Polyethylene oxide (PEO) [15, 16], poly(vinylidene fluoride) (PVDF) [17], poly(methyl methacrylate) (PMMA) [18, 19], and poly(vinyl alcohol) (PVA) [20] have been studied as gel polymer matrices. Among these polymers, PVDF is mainly used as a semicrystalline polymer with relatively good mechanical properties, excellent swelling characteristics, high dielectric constant, and thermal stabilities [17], which has been applied to various applications [21, 22]. However, the dense pore structure of the pristine PVDF membrane restricts the application for the separator in LIBs. In addition, the low ionic conductivity hampered by the high crystallinity of PVDF is also an obstacle. Furthermore, the presence of the strong polar C–F bond deteriorates the compatibility between PVDF and

✉ Jiuqing Liu
jiuqing_liu@163.com

[1] School of Metallurgy and Environment, Central South University, Changsha 410083, Hunan, China

lithium, resulting in the increase in interfacial impedance. Therefore, researchers focus on the preparation of new polymer electrolyte by means of blending different polymers [23–25], innovative polymer synthesis [26, 27], and synthesis of composite polymer electrolytes by addition of inorganic fillers [28, 29]. Of the mentioned techniques, blending has been identified as a simple and effective method due to the ease of preparation and property control. Kondawar et al. prepared PVDF/P(VC-VAc) blending polymer electrolytes for lithium-ion battery with $LiNi_{0.5}Mn_{1.5}O_4$ as cathode and showed ionic conductivity at 3.57 mS cm^{-1} [22]. Zuo et al. developed an ultra-thin PVDF/HEC blending polymer coating layer for modifying th ePE separator with superior cycling stability and ionic conductivity at room temperature [26].

As a hydrophilic substance, PMMA has good compatibility with liquid electrolyte and can improve the affinity between the separator and the electrolyte, thereby improving the electrolyte absorption and ionic conductivity of the separator. A polymer electrolyte composed of PVDF, PMMA, $LiClO_4$, and DMP exhibited the ionic conductivity of about 4.2 mS cm^{-1} at 30 °C [30]. Yvonne et al. investigated the PVDF/PMMA membranes' properties with the addition, of CA and the result exhibited the decreased crystallinity due to the addition of CA, the highest porosity of 99.1%, and melting temperature at 162 °C [23]. Numerous studies [31–33] have also reported the application of polymer blending in battery separators. Binary blending in the range of blend compatibility can exploit the advantages of polymer materials and may produce new properties. Therefore, a blending membrane based on PVDF/PMMA polymer is prepared to optimize membrane performance.

In the paper, the PVDF/PMMA blending membrane for lithium-ion batteries was developed and fabricated by the non-solvent-induced phase separation (NIPS) method. PVDF/PMMA blending membranes with varied weight ratios were applied to investigate the effect of PMMA on LIB performance, mainly including its compatibility with lithium, morphology, ionic conductivity, thermal stability, and cycle performance.

Experimental

Materials

PVDF (HSV900) was obtained from Arkema Chemical Co., Ltd., and PMMA (5LX-40, M_w = 200,000 g mol^{-1}) was purchased from Longxin Chemical Co., Ltd. (Heilongjiang Province, China). Dimethylacetamide (DMAc) was obtained from Guangdong Guanghua Tech. Co., Ltd., China. The liquid electrolyte was 1.0 M $LiPF_6$ in ethylene carbonate (EC)/dimethyl carbonate (DMC)/ethyl methyl carbonate (EMC) ($M_{EC}/M_{DMC}/M_{EMC}$: = 1:1:1) (Suzhou Ganmin Chemical Reagent Co., Ltd., China). A commercial PP/PE/PP composite separator (Celgard 2320) was regarded as a contrast with the thickness of 20 μm.

Blending membrane preparation

The poly(vinylidene fluoride) (PVDF)/polymethyl methacrylate (PMMA) blending membrane was prepared by the non-solvent-induced phase separation (NIPS) method. PVDF and PMMA were dissolved into dimethylacetamide (DMAc) with the mass ratio M_{PVDF}/M_{PMMA} = 10:0, 9:1, 8:2, 6:4, respectively, and the total mass percentage of the PVDF/PMMA polymer in the casting solution was 12%. The slurry was stirred in the oil bath at 70 °C for 24 h, then the solution was placed in a vacuum oven for 48 h to eliminate the tiny bubble. After that, the slurry was casted on a glass plate by using a doctor blade and immersed into a coagulation bath (deionized water), then the resulting blending membrane (thickness 70–80 μm) was further immersed into deionized water to remove residual organic solvent for 48 h. Finally, it was air-dried and placed in the vacuum oven. The blending membranes with a mass ratio of PVDF/PMMA = 10:0, 9:1, 8:2, and 6:4 in this paper are denoted as PM-0, PM-1, PM-2, and PM-3, respectively.

Blending compatibility

There are differences among various polymers as for the ability to form a homogeneous system in two or more blends, and the mutual solubility between polymers can be defined by the concept of compatibility [34, 35]. According to Gibbs energy ($\Delta G_m = \Delta H_m - T\Delta S_m$), the mixing process can only proceed spontaneously when the value of the mixed Gibbs free energy is less than zero under normal pressure. The blending components tend to diffuse to each other to achieve a uniform mixture when the compatibility between the blending components is excellent [36].

Based on the concept of material solubility parameter, Bohn [37] proposed the notion of the polymer solubility parameter used to characterize the strength of interaction between simple liquid molecules as in Eq. (1):

$$\delta = (\Delta E/V_1)^{1/2} \quad (1)$$

where V_1 is the molecular volume of liquid molecule, ΔE is the intermolecular cohesive energy, δ is the material solubility parameter.

Bernard [38] optimized the polymer solubility parameter theory, and there is usually no specific interaction between the blending components, resulting in a low mixing entropy of the blending system [39]; accordingly, the mixed enthalpy can be a substitute for the mixed Gibbs free energy to predict

the degree of blend between the various components of the polymer. ΔH_m (J cm^{-3}) is calculated by Eq. (2):

$$\Delta H_m = \left\{ X_1 M_1 \rho_1 (\delta_1 - \delta_2)^2 \left[\frac{X_2}{X_1 M_2 \rho_2 + X_2 M_1 \rho_1} \right]^2 \right\}^{1/2} \quad (2)$$

where X_1 and X_2 are the mass fractions of polymers 1 and 2, respectively ($X_1 + X_2 = 1$), M_1 and M_2 are the relative molecular masses (g mol^{-1}) of the polymer monomer, respectively, ρ_1 and ρ_2 are the corresponding polymer densities (g cm^{-3}), respectively, and δ_1 and δ_2 are the solubility parameters of the polymer, respectively.

A large number of experimental data show that [40, 41], when the mixed enthalpy is less than 0.0418 J cm^{-3}, such a binary blend system can be regarded as a compatible system.

Characterization

The surface morphologies of PVDF/PMMA blending membranes were observed through a scanning electron microscope (SEM, JSM5600L, Japan).

The ionic conductivity (σ, mS cm^{-1}) of the membrane was evaluated by an AC impedance spectroscopy of symmetrical battery in order to eliminate the effects of cathode and anode impedance with frequency ranging from 10^{-2} Hz to 10^6 Hz over 5 mV of AC amplitude. The ionic conductivity is calculated from Eq. (3):

$$\sigma = l/(R_b \times A) \quad (3)$$

where R_b is the membrane bulk impedance, and A and l are the effective area and thickness of the membrane, respectively.

The connection between ionic conductivity and temperature can be depicted by Arrhenius equation as shown in Eq. (4):

$$\sigma = \delta_0 \exp(-E_a/RT) \quad (4)$$

where δ_0 means the preexponential factor, E_a is the activation energy, and T and R are the temperature and molar gas constant, respectively.

In addition, the thermal stability of the PVDF/PMMA blending membrane was analyzed through DTA (differential thermal analysis, SDT-Q600) from 100 to 600 °C at a heating rate of 10 °C min^{-1} in a nitrogen atmosphere. Besides, the dimensional changes were observed after heating at 25 °C, 100 °C, and 160 °C for 30 min. The thermal shrinkage ratio (TSR) was calculated by Eq. (5):

$$\mathrm{TSR}\ (\%) = (s_0 - s)/s_0 \times 100\% \quad (5)$$

where s_0 and s represent the area of the separator before and after thermal treatment, respectively.

The electrochemical stability was examined by running linear sweep voltammetry (LSV) from 3.0 to 6.0 V at a scan rate of 1 mV s^{-1}. Lithium metal and stainless steel act as counter and working electrodes, respectively. The electrolyte contact angles were measured on a contact angle meter (JGW360, Chengde Chenghui Testing Equipment Co., Ltd., China) by the sessile drop method with 5 μL of electrolyte. Crystal structures of the separators were investigated by X-ray diffraction (XRD, RINT-2000, Japan).

The $LiCoO_2$/electrolyte/Li half-cells were assembled in an argon-filled glove box with oxygen partial pressure less than 1 ppm and sealed in CR2025 coin cells. The $LiCoO_2$ cathode was prepared by blending 80 wt% $LiCoO_2$ (Hunan Shanshan

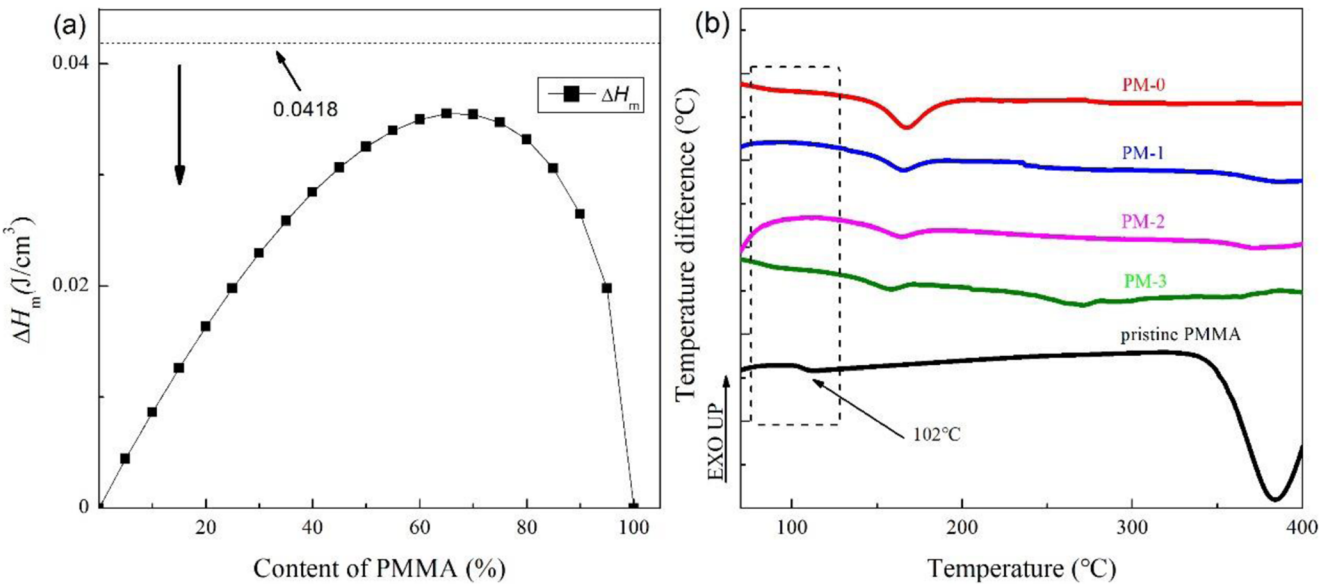

Fig. 1 **a** Variation of mixing enthalpy with PMMA content in the PVDF/PMMA blending system. **b** DTA analyses of pristine PMMA and PVDF/PMMA blending membranes

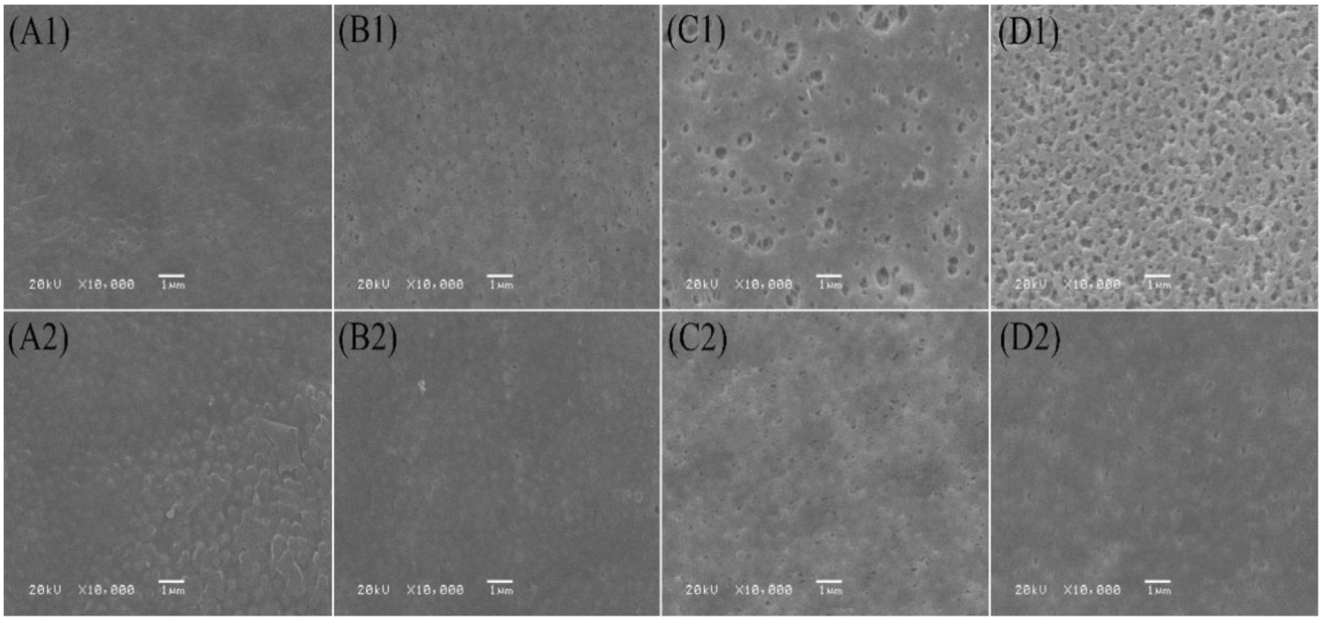

Fig. 2 SEM image of the top view: **A1** PM-0, **B1** PM-1, **C1** PM-2, and **D1** PM-3 membranes, bottom view: **A2** PM-0, **B2** PM-1, **C2** PM-2, and **D2** PM-3 membranes

Battery Materials Co., Ltd., China), 10 wt% PVDF as binder (Arkema, M_w = 1,000,000 g mol^{-1}), and 10 wt% carbon black (Super P, Timcal). NMP was added as solvent for wet grinding, and the wet-milled cathode slurry was uniformly coated on an aluminum foil and transferred to a vacuum oven for 24 h, then the dried coated cathode material was cut into a wafer of a specified size by a punching machine and stored in a vacuum oven.

Results and discussions

Miscibility characterization

The mixed enthalpy of the PVDF/PMMA blending system is calculated through Eq. (2) to predict polymer blending. As shown in Fig. 1a, the mixing enthalpy tends to increase gradually and then decrease with the addition of more PMMA, but the value of mixed enthalpy is always lower than 0.0418 J cm^{-3}. It can be seen that the PVDF and PMMA polymers are completely compatible in the blending ratio range from the above discussions. Apart from that, the DTA analyses of glass transition temperatures shown in Fig. 1b also demonstrate the compatibility of polymers. The glass transition temperature (T_g) is the characteristic temperature of amorphous polymer. T_g of pristine PMMA is actually measured to be 102 °C from Fig. 1b while that of PVDF is − 35 °C [42]. So it is difficult to observe the change of T_g in a large interval from Fig. 1b. It should be noted that the shift of the T_g peak is small even under the condition of blending and the DTA curves of PVDF/PMMA blending membranes exhibit no endothermic peak near 102 °C as seen in Fig. 1b, suggesting that there is no crystal phase of PMMA in the PVDF/PMMA blending membrane and the PMMA molecular chain is well dispersed [25].

Morphological characterization

Figure 2 shows SEM images of the PVDF/PMMA blending membrane which reflect their pore size and distribution. The top surface of the pristine PVDF membrane has a small pore structure with a pore diameter less than 200 nm seen from Fig. 2(A1). As shown in Fig. 2(A1–D1), the pores on the top surfaces of the PVDF/PMMA blending membranes gradually become larger and much more porous as the weight ratio of PMMA increases. So it would appear that the morphology of the PVDF/PMMA blending membrane exhibits the most

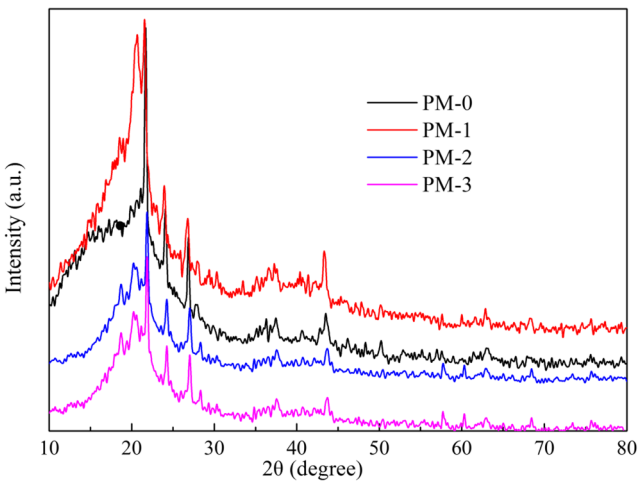

Fig. 3 XRD patterns of PM-0, PM-1, PM-2, and PM-3 membranes

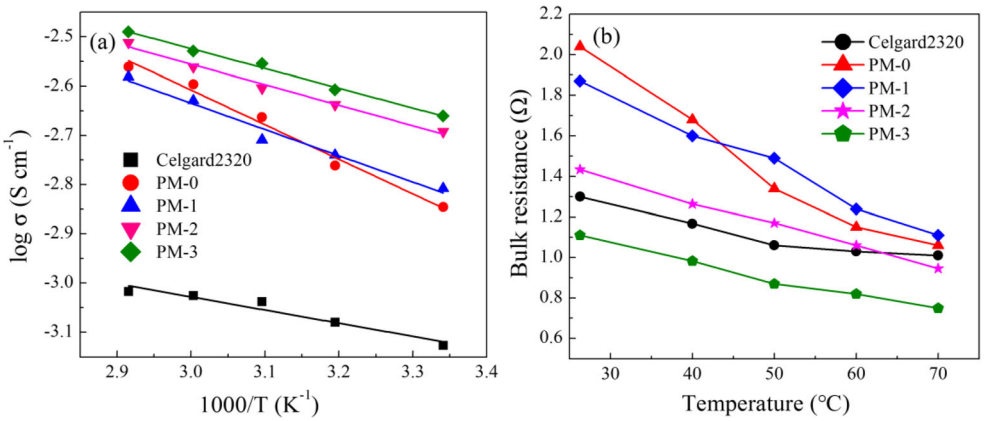

Fig. 4 **a** Ion conductivity curves of PM-0, PM-1, PM-2, and PM-3 membranes and the Celgard 2320 separator at different temperatures. **b** The corresponding bulk impedance change at different temperatures

obvious variety when the PMMA ratio reaches 40% and displays a cross-linked pore structure conducive to the passage of lithium-ions. On the other hand, the bottom surface of the pristine PVDF membrane from Fig. 2(A2) possesses the dense structure and spherical crystals with good crystallinity, which can be ascribed to the slow exchange process of solvent and non-solvent. Contrary to the change in pore size and porosity, the crystallinity of the PVDF/PMMA blending membrane decreases with the increase in PMMA content. It can be seen from the phenomenon that minor pores begin to appear at the bottom of the blending membrane and the spherical crystal disappears. However, the proportion of PMMA cannot be increased

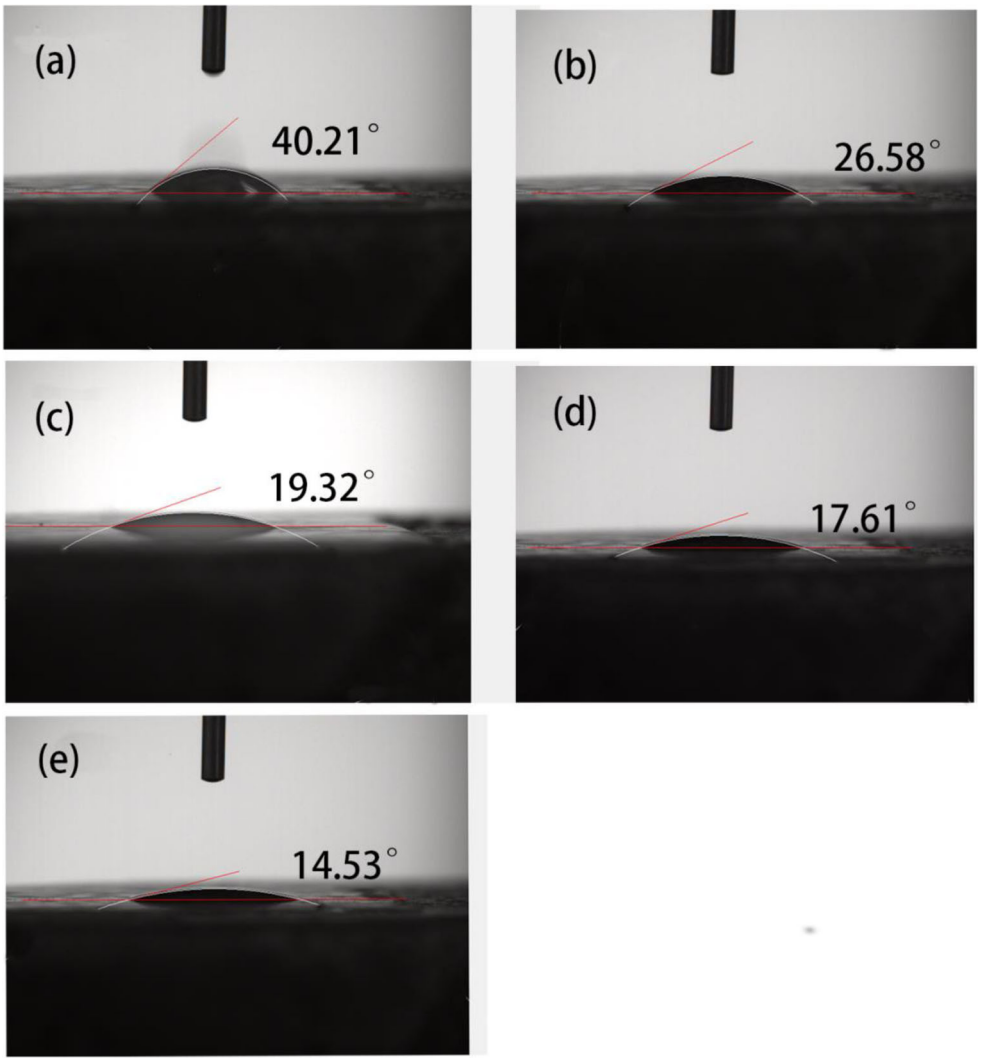

Fig. 5 Contact angle photographs of the **a** Celgard 2320 separator and **b** PM-0, **c** PM-1, **d** PM-2, and **e** PM-3 membranes

indefinitely; PMMA is commonly known as plexiglass with a certain degree of brittleness. Therefore, this study explores that the optimal upper limit of the PMMA mixing ratio is 40%.

X-ray diffraction characterization

The X-ray diffraction pattern helps to provide the effect of PMMA on the structure and crystallization of PVDF in the sample. As shown in Fig. 3, in the case of the pristine PVDF (PM-0) membrane, diffraction peaks at about 18.7° and 26.6° are ascribed to α-PVDF [43]. The presence of a sharp peak at 21.6° and a small peak around 36.8° confirms the formation of the β-phase [44]. It is noted that these peaks have been suppressed when PMMA was added in the PVDF membranes, indicating a significant crystallinity decrease in the PVDF/PMMA blending membranes. Therefore, the PVDF/PMMA blending membranes become more amorphous with higher ionic conductivity.

Ionic conductivity

Figure 4a shows the temperature-dependent ionic conductivity. It is evident that the rise in temperature contributes to the improvement in electrolyte conductivity from Fig. 4a which may be due to the promotion on thermal movement of ions and polymer chains by the volume expansion of the polymer during heating [45]. Calculated in Eq. (4), the corresponding ionic conductivity of the Celgard 2320 separator and PM-0, PM-1, PM-2, and PM-3 membranes at 26 °C are 0.84, 1.43, 1.55, 2.03, and 2.18 mS cm^{-1}, respectively. It is clearly seen that the ionic

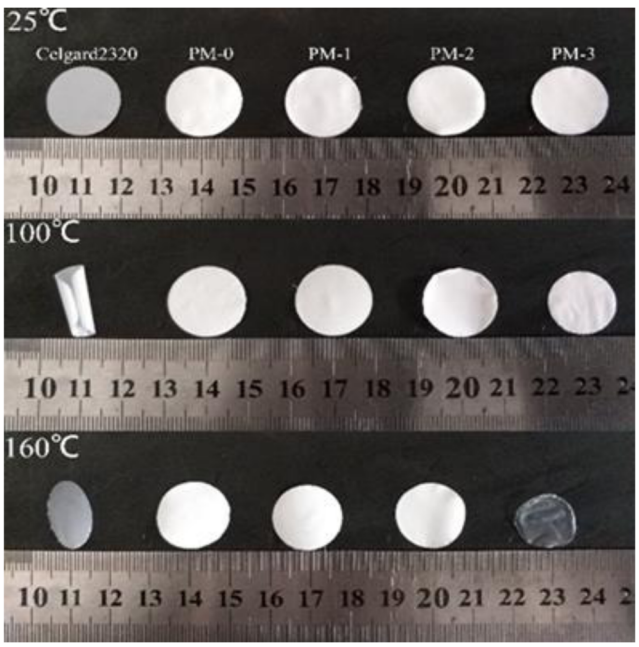

Fig. 6 Photographs of the Celgard 2320 separator and the PM-0, PM-1, PM-2, and PM-3 membranes before and after heat treatment at 25 °C, 100 °C, and 160 °C for 30 min

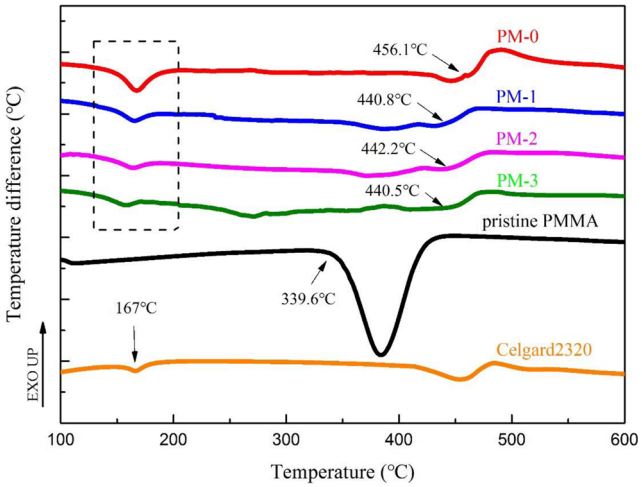

Fig. 7 DTA analyses of pristine PMMA, Celgard 2320 separator, and PM-0, PM-1, PM-2, and PM-3 membranes

conductivity of the PVDF/PMMA polymer electrolyte is significantly superior to that of the Celgard 2320 separator. In terms of bulk impedance, the bulk impedance of the membranes decreases with the increase in temperature as shown in Fig. 4b, in which the bulk impedance of the PM-3 membrane (1.11 Ω) is even smaller than that of the Celgard 2320 separator (1.30 Ω) at room temperature, while the thickness of the PM-3 membrane is more than three times that of the Celgard 2320 separator. Therefore, the PM-3 membrane owns excellent ability to conduct ion on account of the participation of PMMA. The effect of PMMA can be summarized as three main reasons [46]: first, the addition of PMMA has an impact on the porous structure and lithium-ion permeability of the PVDF/PMMA blending membrane. Moreover, the crystallinity of PVDF reduces due to the addition of PMMA. Last but not least, the strong interaction between carbonyl in PMMA and oxygen-containing functional groups in carbonate solvents results in better compatibility between membrane and electrolyte, which strengthens the ion conductivity of the non-crystalline region [46].

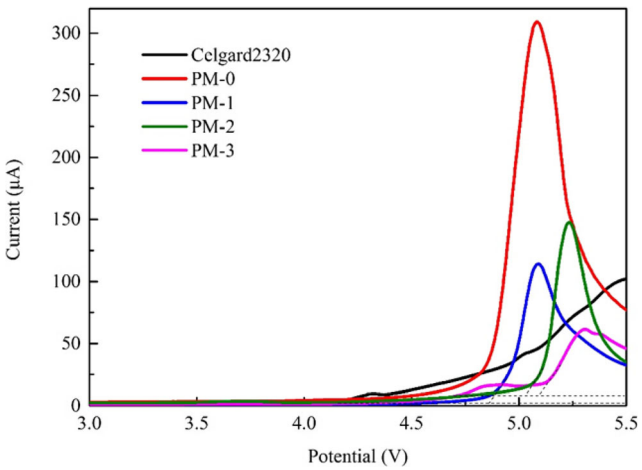

Fig. 8 Electrochemical stability window of the Celgard 2320 separator and PM-0, PM-1, PM-2, and PM-3 membranes

Wettability analysis

The separator with good affinity to the electrolyte can significantly improve the electrochemical performance of the battery. Herein, the wettability of the separator is investigated using contact angle measurements; as shown in Fig. 5, the electrolyte contact angle is 40.21° for the Celgard 2320 separator and 14.53° for the PM-3 membrane. Obviously, the PVDF/PMMA blending membranes have better wettability with the addition of PMMA, which can be ascribed to better compatibility the between membrane and electrolyte resulting from the strong interaction between carbonyl in PMMA and oxygen-containing functional groups in carbonate solvents [46].

Thermal stability

Figure 6 compares the dimensional stability of the Celgard 2320 separator with those of the prepared PVDF/PMMA blending membranes at 25 °C, 100 °C, and 160 °C for 30 min. It is worth noting that the shrinkage rates of PM-0, PM-1, PM-2, and PM-3 membranes at 160 °C are 10.3%, 15.2%, 18.1%, and 37.8%, respectively. When the PMMA content reaches 40%, the PM-3 membrane exhibits a reflow phenomenon. Nevertheless, the Celgard 2320 separator shrinks severely at 160 °C owing to the lower melting point of PE materials. Therefore, it can be considered that the PVDF/PMMA blending membrane exceeds the Celgard

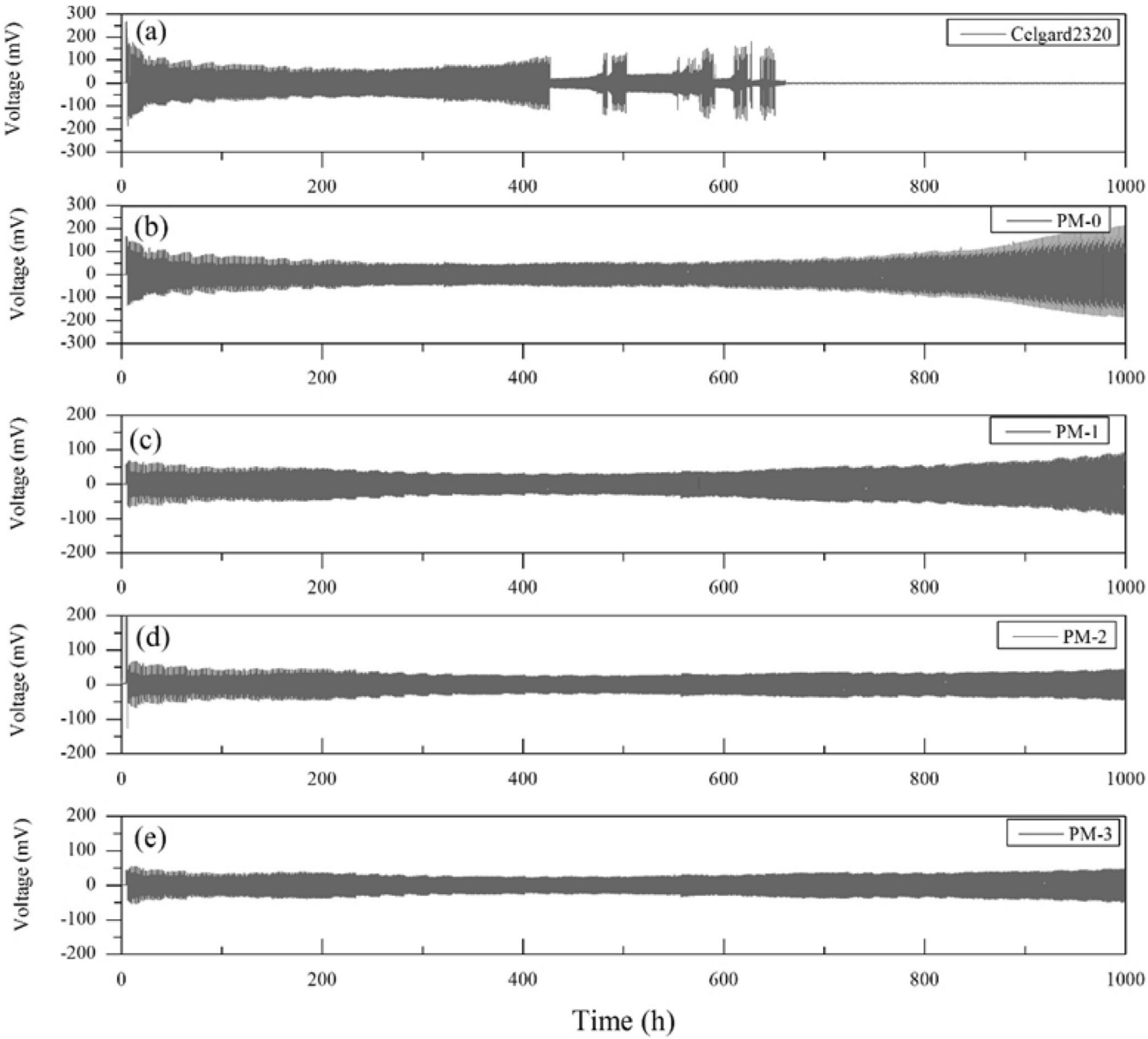

Fig. 9 Polarization cycle chart of Li/electrolyte/Li cells using the Celgard 2320 separator (**a**) and PM-0 (**b**), PM-1 (**c**), PM-2 (**d**), and PM-3 membranes (**e**)

2320 separator concerning thermal stability. As presented in Fig. 7, DTA analyses were also performed to investigate thermal stability of PVDF/PMMA blending membranes and the Celgard 2320 separator. The melting endotherm peaks of PM-0, PM-1, PM-2, and PM-3 membranes emerge at 165.0, 164.0, 163.0, and 157.0 °C, respectively. It is obviously observed that the T_m (melting temperature) of the PVDF/PMMA blending membrane decreases with the increase in PMMA content, which means a slight decrease in dimensional stability for the blending membranes. Furthermore, the melting endothermic peak area of blending membranes gradually reduces with more PMMA existing, which indicates fewer crystal phases as well as the decrease in crystallinity of the PVDF/PMMA blending membrane. As for the exothermic peaks corresponding to decomposition of the blending membrane, the initial decomposition temperatures for PM-0, PM-1, PM-2, and PM-3 membranes in Fig. 7 are observed at 456.1, 440.8, 442.2, and 440.5 °C, respectively, while pristine PMMA has an endothermic decomposition peak at 339.6 °C. The result suggests that the addition of PMMA reduces the thermal decomposition temperature of the PVDF/PMMA blending membrane.

Electrochemical stability

The electrochemical stability of the PVDF/PMMA blending membrane was characterized by LSV, as shown in Fig. 8, in which forward voltage scanning was performed on Li/electrolyte/SS asymmetric cells at a rate of 1 mV s^{-1}. As the upper limit of electrolyte stability range, the decomposition initiation voltage is generally located at the intersection of the extrapolated linear current in the high-voltage region with the voltage axis [47]. For the Celgard 2320 separator, there is an anodic peak onset at 4.3 V resulting from the decomposition of carbonate solvent. When PMMA is blending with the PVDF polymer matrix, the PVDF/PMMA blending membranes exhibit a higher decomposition voltage up to 4.5 V (PM-0), 4.8 V (PM-1), 5.0 V (PM-2), and 4.7 V (PM-3) than 4.3 V for the Celgard 2320 separator, indicating that the electrochemical stability of prepared separators is suitable for the normal application in LIBs. The enhanced electrochemical stability, on the one hand, may be due to the low crystallinity of PMMA. Besides, the absorption of a large amount of lithium salt solvent in the amorphous phase slows the excessive oxidation of the carbonate solvent [48].

Compatibility with lithium

In order to investigate the capability of the electrolyte to eliminate polarization in the dynamic cycle, the polarization experiment of the polymer membrane in Li/Li symmetrical cells (charge time/discharge time = 1 h/1 h, current density 0.5 mA cm^{-2}) was performed as illustrated in Fig. 9. Lithium-symmetric batteries do not undergo cyclic short-circuiting when employing PM-0, PM-1, PM-2, and PM-3 membranes, while the Celgard 2320 separator eventually gets short-circuited due to the growth of lithium dendrites. The internal polarization leads to the increase in potential difference as the cycle goes on from Fig. 9. Figure 10a and b show the polarization curves of the interception period 300–310 h in the middle of the cycle and 990–1000 h in the end of the cycle. At 300 h, the voltages centered at 62.5, 45.0, 34.0, 31.0, and 28.0 mV are obviously observed for symmetric cells using the Celgard 2320 separator and PM-0, PM-1, PM-2, and PM-3 membranes, respectively. The lower potential difference plateau means the smaller degree of polarization. Besides, it

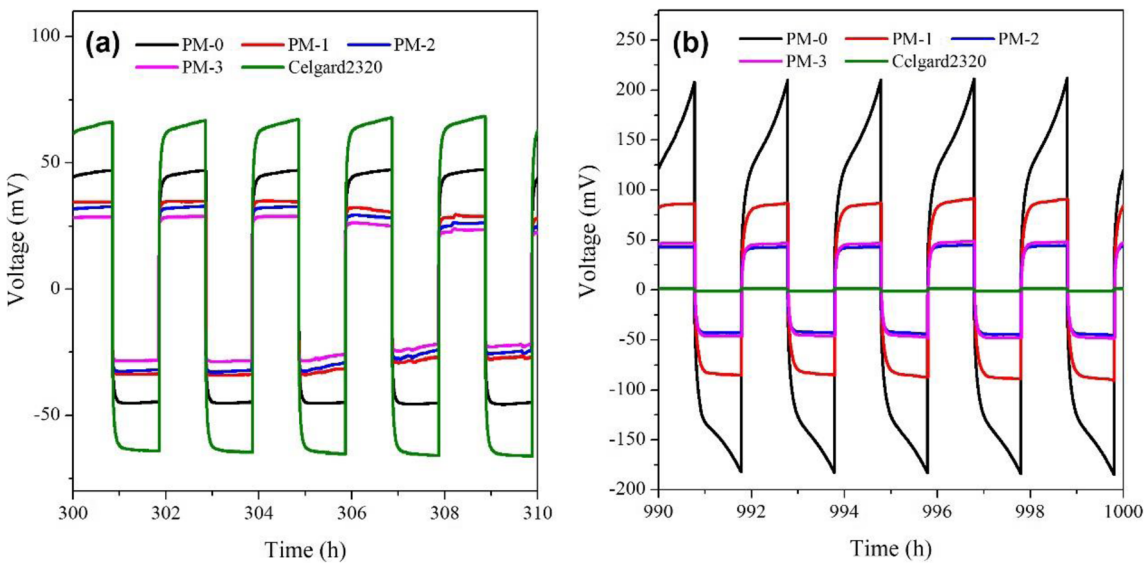

Fig. 10 Polarization platform curve at 300–310 h (**a**) and 900–1000 h (**b**)

contributes to the better interface compatibility between the separator and lithium. Concluded from the above discussion, the addition of PMMA improves the compatibility of the separator with lithium. Moreover, at the end of the cycle (990 h), the polarization voltages of symmetric batteries using the Celgard 2320 separator and the PM-0, PM-1, PM-2, and PM-3 membranes turn into 0, 124.0, 86.0, 42.0, and 46.0 mV, respectively, in which the Celgard 2320 separator is short-circuited owing to the piercing of lithium dendrites, resulting in zero voltage. Due to the relatively dense pore structure and low ionic conductivity of the membrane, the polarization inside the cell with the PM-0 membrane gradually aggravates, which leads to the maximum polarization potential difference. In contrast, the PM-1, PM-2, and PM-3 membranes possess excellent ionic conductivity and low interfacial impedance, thus resulting in the minor internal polarization of cells.

Cell cycle performance

Figure 11a–e present the 1st, 100th, and 200th charge–discharge profiles of $LiCoO_2$/electrolyte/Li half-cells with different separators, by which the cell polarization condition is reflected. The charge–discharge plateaus of the Celgard 2320 cell becomes inclined with significant difference, suggesting severe polarization and poor cycle stability. However, the voltage difference of cells assembled with PVDF/PMMA blending membranes slightly increases, which implies an efficient reaction process and excellent cycle stability. This conclusion represents better cycling

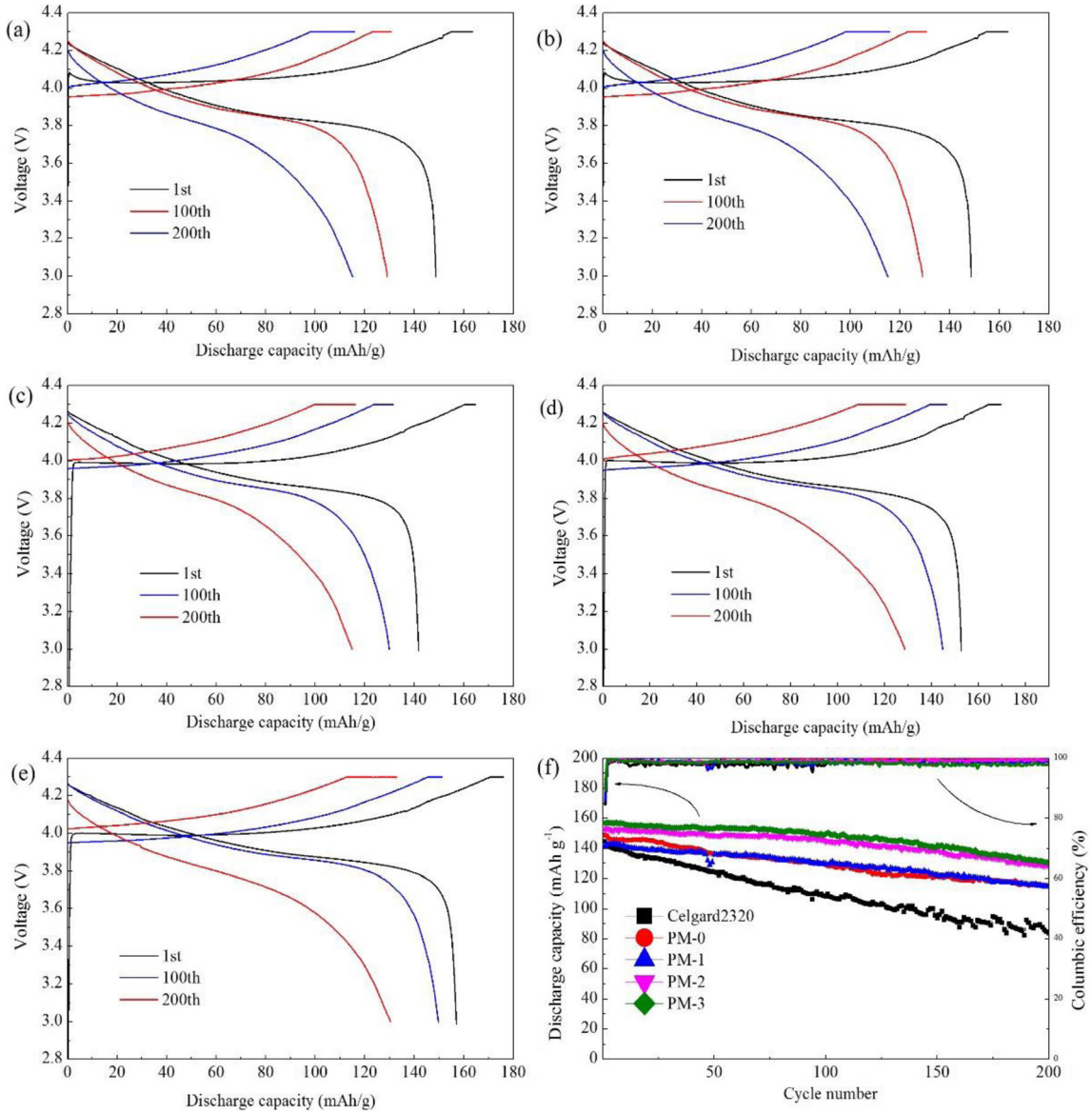

Fig. 11 Charge–discharge profiles of the cells at 1 C with the **a** Celgard 2320 separator and **b** PM-0, **c** PM-1, **d** PM-2, **e** PM-3 membranes, and **f** cycling stability of the cells at 1 C

performance for the cells assembled with PVDF/PMMA blending membranes. Moreover, the slow increase in voltage difference between the charge–discharge plateaus of cells employing blending membranes can be considered as normal capacity decay. Apart from that, the cycling performance of the cells based on the Celgard 2320 separator and PVDF/PMMA blending membranes at room temperature under the rate of 1 C can be further compared in Fig. 11f. After 200 cycles, their specific capacities are 83.6, 114.0, 115.1, 128.5, and 130.7 mAh g^{-1}, which belong to the Celgard 2320 separator and the PM-0, PM-1, PM-2, and PM-3 membranes, respectively. It is obvious that the charge–discharge cycling performance of cells with PVDF/PMMA blending membranes is superior to cells with the Celgard 2320 separator. This result can be attributed to the improvement in ionic conductivity and interfacial compatibility. Meanwhile, the columbic efficiency values are close to 100%, which means very low capacitance recession.

The rate capabilities of cells based on the Celgard 2320 separator and PVDF/PMMA blending membranes were measured by applying various discharge current densities ranging from 0.2 to 4.0 C every 5 cycles. As seen in Fig. 12, the discharge-specific capacity of cells decreases with the increase in discharge current density. However, among cells with the Celgard 2320 separator and PVDF/PMMA blending membranes, the cell with the PM-3 membrane performs the best discharge-specific capacity at any rate, especially 4 C, at which the specific discharge capacities are 101.8, 105.9, 126.1, 119.6, and 133.3 mAh g^{-1} for the Celgard separator and the PM-0, PM-1, PM-2, and PM-3 membranes, respectively. Consequently, the above results indicate that the PM-3 membrane possesses excellent electrochemical performances. Therefore, it could be a promising separator for the applications in lithium-ion batteries.

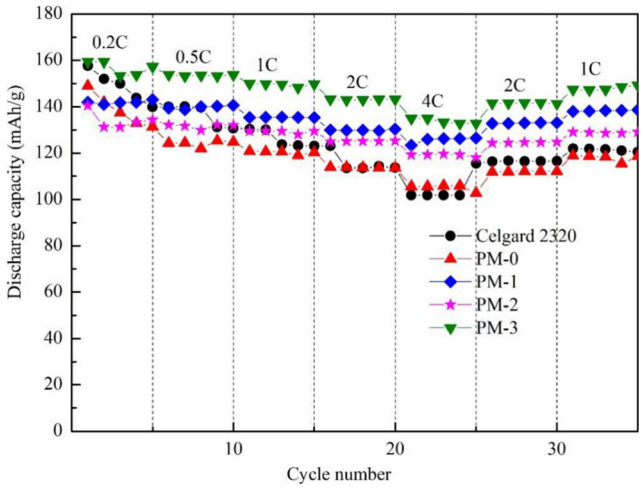

Fig. 12 Cycle curves of the Celgard 2320 separator and the PM-0, PM-1, PM-2, and PM-3 membranes

Conclusions

This work has presented a gel polymer electrolyte based on PVDF/PMMA blending which are fabricated via the non-solvent phase separation method from the perspective of polymer blending compatibility. The blend of PMMA and PVDF can significantly change the surface morphology of initial membranes, resulting in a dense layer of the PVDF/PMMA blending membrane porous, better compatibility, and enhancement of the ion-conducting ability in the amorphous region. Although the addition of PMMA results in poor performance of PVDF/PMMA blending membranes in terms of thermal stability, it must be noted that PMMA enhances the electrochemical stability of the membrane. Meanwhile, the interface stability between the PVDF/PMMA blending membrane and lithium is also improved. Finally, the specific capacity of the cell assembled with the PM-3 membrane can reach 130.7 mAh g^{-1} after circulating 200 cycles at the rate of 1 C, which performs better than that with the Celgard 2320 separator. Consequently, the PVDF/PMMA blending membrane can be applied as a promising separator for rechargeable lithium-ion batteries.

Funding information This study was supported by the National Key R&D Program of China (Grant No. 2018YFB0104200).

References

1. Arora P, Zhang ZM (2004) Battery separators. Chem Rev 104: 4419–4462
2. Zhang SS (2007) A review on the separators of liquid electrolyte Li-ion batteries. J Power Sources 164:351–364
3. Zhang H, Zhou MY, Lin CE, Zhu BK (2015) Progress in polymeric separators for lithium ion batteries. RSC Adv 5:89848–89860
4. Cho TH, Tanaka M, Ohnishi H, Kondo Y, Yoshikazu M, Nakamura T, Sakai T (2010) Composite nonwoven separator for lithium-ion battery: development and characterization. J Power Sources 195:4272–4277
5. Lee H, Alcoutlabi M, Watson JV, Zhang X (2013) Polyvinylidene fluoride-co-chloro-trifluoroethylene and polyvinylidene fluoride-co-hexafluoropropylene nanofiber-coated polypropylene microporous battery separator separators. J Polym Sci B Polym Phys 51:349–357
6. Lee H, Alcoutlabi M, Toprakci O, Xu GJ, Watson JV, Zhang X (2014) Preparation and characterization of electrospun nanofiber-coated separator separators for lithium ion batteries. J Solid State Electrochem 18:2451–2458
7. Cui JQ, Liu JQ, He CF, Li J, Wu XF (2017) Composite of polyvinylidene fluoride–cellulose acetate with $Al(OH)_3$ as a separator for high-performance lithium ion battery. J Membr Sci 541:661–667
8. Lee H, Jeon H, Gong S, Ryou MH, Lee YM (2018) A facile method to enhance theuniformity and adhesion properties of water-based ceramic coating layers on hydrophobic polyethylene separators. Appl Surf Sci 427:139–146
9. Zhao XX, Zhang ZL, Yang SS, Liang GC (2017) Inorganic ceramic fiber separator for electrochemical and safety performance improvement of lithium ion batteries. Ceram Int 43:14775–14783
10. Zhang ZY, Lai YQ, Zhang ZA, Zhang K, Li J (2014) Al_2O_3-coated porous separator for enhanced electrochemical performance of lithium sulfur batteries. Electrochim Acta 129:55–61

11. Wang GC, Lai YQ, Zhang ZA, Li J, Zhang ZY (2015) Enhanced rate capability and cycle stability of lithium-sulfur batteries with a bifunctional MCNT@PEG-modified separator. J Mater Chem A 3:7139–7144
12. He CF, Liu JQ, Li J, Zhu FF, Zhao HJ (2018) Blending based polyacrylonitrile/poly (vinylalcohol) separator for rechargeable lithium ion batteries. J Membr Sci 560:30–37
13. Li WL, Wu YH, Wang JW, Huang D, Chen LZ, Yang G (2015) Hybrid gel polymer electrolyte fabricated by electrospinning technology for polymer lithium-ion battery. Eur Polym J 67:365–372
14. Cheng XL, Pan J, Zhao Y, Liao M, Peng HS (2018) Gel polymer electrolytes for electrochemical energy storage. Adv Energy Mater 8(7):1702184
15. Jinisha B, Anilkumar KM, Manoj M, Pradeep VS, Jayalekshmi S (2017) Development of a novel type of solid polymer electrolyte for solid state lithium battery applications based on lithium enriched poly (ethylene oxide) (PEO)/poly (vinyl pyrrolidone) (PVP) blend polymer. Electrochim Acta 235:210–222
16. Dias FB, Plomp L, Veldhuis JBJ (2000) Trends in polymer electrolytes for secondary lithium batteries. J Power Sources 88:169–191
17. Liu LP, Wang Z, Zhao ZK, Zhao YJ, Li F, Yang LB (2016) PVDF/PAN/SiO_2 polymer electrolyte separator prepared by combination of phase inversion and chemical reaction method for lithium ion batteries. J Solid State Electrochem 20:699–712
18. Chen HW, Lin TP, Chang FC (2002) Ionic conductivity enhancement of the plasticized PMMA/$LiClO_4$ polymer nanocomposite electrolyte containing clay. Polymer 43:5281–5288
19. Kahn WS, Asmatulu R, Rodriguez V, Ceylan M (2014) Enhancing thermal and ionic conductivities of electrospun PAN and PMMA nanofibers by graphene nanoflake additions for battery-separator applications. Int J Energy Res 38:2044–2051
20. Subramania A, Sundaram NTK, Kumar GV, Vasudevan T (2006) New polymer electrolyte based on (PVA-PAN) blend for Li-ion battery applications. Ionics 12:175–178
21. Dandekar MP, Itankar SG, Kondawar SB, Nandanwar DV, Koinkar P (2018) Photoluminescent electrospun europium complex $Eu(TTA)_3$phen embedded polymer blends nanofibers. Opt Mater 85: 483–490
22. Mahant YP, Kondawar SB, Nandanwar DV, Koinkar P (2018) Poly (methyl methacrylate) reinforced poly (vinylidene fluoride) composites electrospun nanofibrous polymer electrolytes as potential separator for lithium ion batteries. Mater Renew Sustain Energy 7:5
23. Yvonne T, Zhang CY, Zhang CH, Omollo E, Ncube S (2014) Properties of electrospun PVDF/PMMA/CA membrane as lithium based battery separator. Cellulose 21:2811–2818
24. Liang YZ, Cheng SC, Zhao JM, Zhang CH, YP Q (2013) Preparation and characterization of electrospun PVDF/PMMA composite fibrous membranes based separator for lithium-ion batteries. Adv Mater Res 122:750–752
25. Idris NH, Rahman MM, Wang JZ, Liu HK (2012) Microporous gel polymer electrolytes for lithium rechargeable battery application. J Power Sources 201:294–300
26. Ma XD, Zuo XX, Wu JH, Deng X, Xiao X, Liu JS, Nan JM (2018) Polyethylene-supported ultra-thin polyvinylidene fluoride/hydroxyethyl cellulose blended polymer electrolyte for 5 V high voltage lithium ion batteries. J Mater Chem A 6:1496–1503
27. Zhao MK, Zuo XX, Ma XD, Xiao X, Liu JS, Nan JM (2017) Self-supported PVdF/P(VC-VAc) blended polymer electrolytes for $LiNi_{0.5}Mn_{1.5}O_4$/Li batteries. J Membr Sci 532:30–37
28. Zuo XX, Wu JH, Ma XD, Deng X, Cai JX, Chen QY, Liu JS, Nan JM (2018) A poly(vinylidene fluoride)/ethyl cellulose and amino-functionalized nano SiO_2 composite coated separator for 5 V high-voltage lithium-ion batteries with enhanced performance. J Power Sources 407:44–52
29. Song DY, Xu C, Chen YF, He JR, Zhao Y, Li PJ, Lin W, Fu F (2015) Enhanced thermal and electrochemical properties of PVDF-HFP/PMMA polymer electrolyte by TiO_2 nanoparticles. Solid State Ionics 282:31–36
30. Rajendran S, Mahendran O, Kannan R (2002) Lithium ion conduction in plasticized PMMA–PVdF polymer blend electrolytes. Mater Chem Phys 74:52–57
31. Wu QY, Liang HQ, Gu L, Yu Y, Huang YQ, Xu ZK (2016) PVDF/PAN blend separators via thermally induced phase separation for lithium ion batteries. Polymer 107:54–60
32. Li D, Shi DQ, Yuan ZZ, Feng K, Zhang HM, Li HF (2017) A low cost shutdown sandwich-like composite separator with superior thermo-stability for lithium-ion battery. J Membr Sci 542:1–7
33. Amaral FA, Dalmolin C, Canobre SC, Bocchi N, Rocha-Filho RC, Biaggio SR (2017) Electrochemical and physical properties of poly (acrylonitrile)/poly (vinyl acetate)-based gel electrolytes for lithium ion batteries. J Power Sources 164:379–385
34. Aouachria K, Belhaneche-Bensemra N (2006) Miscibility of PVC/PMMA blends by vicat softening temperature, viscometry, DSC and FTIR analysis. Polym Test 25:1101–1108
35. Bottino A, Capannelli G, Munari S, Turturro A (1988) Solubility parameters of poly (vinylidene fluoride). J Polym Sci B Polym Phys 26:785–794
36. Bohn L (1968) Incompatibility and phase formation in solid polymer mixtures and graft and block copolymers. Rubber Chem Technol 41:495–513
37. Barton AFM (1975) Solubility parameters. Chem Rev 75:731–753
38. Schneier B (1973) Polymer compatibility. J Appl Polym Sci 17:3175–3185
39. Huang YH, Xiao CB (2007) Miscibility and mechanical properties of quaternized polysulfone/benzoyl guar gum blends. Polymer 48: 371–381
40. Small PA (1953) Some factors affecting the solubility of polymers. J Appl Chem 3:71–80
41. Li SW, Cui ZY, Zhang L, He BQ, Li JX (2016) The effect of sulfonated polysulfone on the compatibility and structure of polyethersulfone-based blend separators. J Membr Sci 513:1–11
42. Brandrup J, Immergut EH, Grulke EA, Abe A, Bloch DR (1999) Polymer handbook, 4th edn. Wiley, New York, p 951
43. Padmaraj O, Venkateswarlu M, Satyanarayana N (2014) Characterization and electrochemical properties of P(VdF-co-HFP) based electrospun nanocomposite fibrous polymer electrolyte for lithium battery applications. Electroanalysis 26:2373–2379
44. Ma T, Cui ZY, Wu Y, Qin SH, Wang H, Yan F, Han N, Li JX (2013) Preparation of PVDF based blend microporous membranes for lithium ion batteries by thermally induced phase separation: I. Effect of PMMA on the membrane formation process and the properties. J Membr Sci 444:213–222
45. Helan Flora X, Ulaganathan M, Babu RS, Rajendran S (2012) Evaluation of lithium ion conduction in PAN/PMMA-based polymer blend electrolytes for Li-ion battery applications. Ionics 18: 731–736
46. Nicotera I, Coppola L, Oliviero C, Castriota M, Cazzanelli E (2006) Investigation of ionic conduction and mechanical properties of PMMA-PVdF blend–based polymer electrolytes. Solid State Ionics 177:581–588
47. Jung HR, Ju DH, Lee WJ, Zhang X, Kotek R (2009) Electrospun hydrophilic fumed silica/polyacrylonitrile nanofiber-based composite electrolyte membranes. Electrochim Acta 54:3630–3637
48. Cui ZY, Xu YY, Zhu LP, Wang JY, Xi ZY, Zhu BK (2008) Preparation of PVDF/PEO-PPO-PEO blend microporous membranes for lithium ion batteries via thermally induced phase separation process. J Membr Sci 325:957–963

Publisher's note Springer Nature remains neutral with regard to jurisdictional claims in published maps and institutional affiliations.